JACS
JOURNAL OF THE AMERICAN CHEMICAL SOCIETY
pubs.acs.org/JACS
Article

Controlling the Oxidation State of the Cu Electrode and Reaction Intermediates for Electrochemical CO_2 Reduction to Ethylene

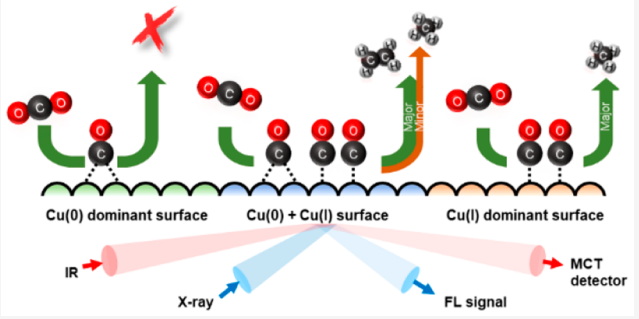
Tsu-Chin Chou, Chiao-Chun Chang, Hung-Ling Yu, Wen-Yueh Yu, Chung-Li Dong, Juan-Jesús Velasco-Vélez, Cheng-Hao Chuang, Li-Chyong Chen, Jyh-Fu Lee, Jin-Ming Chen, and Heng-Liang Wu*

Cite This: J. Am. Chem. Soc. 2020, 142, 2857−2867

Read Online

ACCESS | Metrics & More | Article Recommendations | Supporting Information

ABSTRACT: Understanding the role of the oxidation state of the Cu surface and surface-adsorbed intermediate species in electrochemical CO_2 reduction is crucial for the development of selective CO_2-to-fuel electrocatalysts. In this study, the electrochemical CO_2 reduction mechanism over the Cu catalysts with various oxidation states was studied by using in situ surface-enhanced infrared absorption spectroscopy (SEIRAS), in situ soft X-ray absorption spectroscopy (Cu L-edge), and online gas chromatography measurements. The atop-adsorbed CO (CO_{atop}) intermediate is obtained on the electrodeposited Cu surface which primarily has the oxidation state of Cu(I). CO_{atop} is further reduced, followed by the formation of C_1 product such as CH_4. The residual bridge-adsorbed CO (CO_{bridge}) is formed on the as-prepared Cu surface with Cu(0) which inhibits hydrocarbon formation. In contrast, the CV-treated Cu electrode prepared by oxidizing the as-prepared Cu surface contains different amounts of Cu(I) and Cu(0) states. The major theme of this work is that in situ SEIRAS results show the coexistence of CO_{atop} and CO_{bridge} as the reaction intermediates during CO_2 reduction and that the selectivity of CO_2-to-ethylene conversion is further enhanced in the CV-treated Cu electrode. The Cu catalysts modulated by the electrochemical method exhibit different oxidation states and reaction intermediates as well as electrocatalytic properties.



Downloaded via UNIV OF EXETER on July 13, 2020 at 04:30:28 (UTC).
See https://pubs.acs.org/sharingguidelines for options on how to legitimately share published articles.

INTRODUCTION

Electrochemical CO_2 reduction reaction (CO2RR) is a promising route to convert CO_2 into valuable hydrocarbon fuels and chemical feedstock for sustainable carbon cycles.[1,2] The catalysts capable of electrochemically reducing CO_2 still suffer from many challenges such as short catalyst lifetime, high overpotential, low Faradaic efficiencies (FEs), and poor product selectivity, mainly due to the multiple number of proton-coupled electron transfer steps.[3] The development of efficient and selective catalysts for CO2RR has attracted tremendous attention.[4−6] Among all of the transition metal catalysts explored for CO2RR, copper (Cu) is a promising catalyst to produce hydrocarbons including methane (CH_4) and ethylene (C_2H_4).[7,8] However, bulk Cu electrode exhibits high overpotentials and a lack of product selectivity. Furthermore, metallic Cu is oxidized under air easily.

Various strategies have been used to enhance the performance of CO2RR by modulating the catalytic structure and physical properties of the electrolyte as well as the oxidation state of Cu catalyst.[4,6,9−14] For instance, Cu nanostructures with different particle size, particle morphology, and surface area exert a great impact on the catalytic properties.[9−14] C_2 products are formed over the Cu(100) electrode, while Cu(111) is effective to produce C_1 products,[7,8] suggesting that the facet of Cu catalyst results in different CO_2 reduction mechanisms. The physical properties of electrolyte also play crucial roles in the product selectivity over the Cu electrodes. The electrolyte with different proton concentrations (pH values) influences the protonation step for the production of COOH in CO2RR.[5]

The product selectivity can be enhanced over the oxide-derived Cu catalysts.[11,13,15−18] These Cu-based materials synthesized by the reduction of thermally oxidized Cu,[19] electrodeposited Cu_2O,[20] and oxygen plasma-treated Cu catalysts[13,18] display a higher current density, formation of CO at low overpotentials, and improved FEs of C_2H_4.[18] The effect of the oxide-derived Cu catalysts on the product selectivity has been studied. The grain boundaries in oxide-derived Cu could provide unique surface sites.[21,22] Reske et al.

Received: October 16, 2019
Published: January 20, 2020

ACS Publications
© 2020 American Chemical Society

https://dx.doi.org/10.1021/jacs.9b11126
J. Am. Chem. Soc. 2020, 142, 2857−2867

showed that the low-coordinated atoms formed on the surface of the catalyst behave as the active sites during the oxide reduction.[9] The $Cu^{\delta+}$ sites remaining on the oxide-derived Cu surface have also been suggested to be the active sites for CO2RR.[18,20] To further examine the effect of Cu(I) on the CO_2 reduction mechanism, previous studies reported that Cu(I) sites alone do not improve the efficiencies of CO2RR. The DFT calculations proposed that the synergy between active surface Cu(I) and Cu(0) regions resulting in the adsorption of CO intermediates on different reaction sites is responsible for improving the CO dimerization.[23] However, experimental evidence is needed for the proposed model.

The surface-adsorbed CO intermediates are formed during CO2RR, followed by the dimerization process of CO intermediates, which are generally regarded as the control step for CH_4 and C_2H_4 formation.[5] In situ surface-enhanced infrared absorption spectroscopy (SEIRAS) is a powerful tool for examining the adsorbed intermediates on Cu catalysts.[24−28] As a result of various adsorption sites for the CO molecule, previous studies on the Cu surface mainly focused on the dynamic evolution of adsorbed CO and the formation of adsorbed CO including atop-adsorbed CO and bridge-adsorbed CO.[27,29,30] The atop-adsorbed CO has been recognized as a common intermediate on the Cu surface,[24−28] and the atop-adsorbed CO alone is observed in a variety of experimental conditions such as pH value of electrolyte,[31] and partial pressure of CO_2 (or CO).[25] These Cu electrodes are electrochemically deposited on Au substrate and chemically deposited on a Si prism.[26,32] In contrast, Gunathunge et al. showed that both atop-adsorbed CO and bridge-adsorbed CO can be formed on the chemically deposited Cu thin film in alkaline pH electrolyte and that the bridge-adsorbed CO is inactive during CO2RR.[27] In addition, these CO intermediates are also observed in the electropolished Cu electrode,[30] suggesting that controlling the formation of atop-adsorbed CO and bridge-adsorbed CO on the Cu surface is still challenging. The CO_2 reduction mechanism behind various Cu electrodes is unclear due to the lack of understanding of the oxidation state of Cu accompanied by the formation of CO intermediates.

In this study, we used in situ soft X-ray absorption spectroscopy, in situ SEIRAS, and online gas chromatography (GC) measurements to study the oxidation state of Cu, surface-adsorbed intermediates, and final products during CO2RR. By combining these in situ techniques, we are able to provide the complementary information and elucidate the reaction pathways about the electrochemical CO_2 reduction mechanism on Cu electrodes. Our results show that the amount of Cu(I) and Cu(0) oxidation states in Cu catalysts can be modulated by the electrochemical method. The coexistence of atop-adsorbed CO and bridge-adsorbed CO on the CV-treated Cu surface is observed during CO_2 reduction. The different CO species formed on the Cu electrodes could play crucial roles in the CO_2 reduction mechanism. The prepared Cu electrodes with specific oxidation states influence the formation of CO intermediates and product selectivity during CO2RR.

EXPERIMENTAL SECTION

Chemicals and Electrolyte. $KHCO_3$ (≥99.8%) and $CuSO_4$ (≥99.8%) were purchased from Sigma-Aldrich. Ultrapure H_2SO_4 (98%) and CO_2 (≥99.995%) were purchased from Kanto Chemical Co. and FMI gas Taiwan, respectively. All chemicals were used as received without further purification. Millipore triple-distilled water (18.2 MΩ) was used to prepare solutions. The CO_2-saturated 0.1 M $KHCO_3$ electrolyte with a pH value of 6.8 is prepared by purging CO_2 in 0.1 M $KHCO_3$ electrolyte for 60 min.

Preparation of As-Prepared Cu Electrodes. A Cu thin film with a thickness of ca. 36 nm was prepared using physical vapor deposition (PVD) on the reflecting plane of a hemicylindrical Si prism or Si wafer by a home-built ion beam sputtering system and then transferred into the electrochemical cell immediately for the measurements to avoid Cu oxidation. The thickness of the as-prepared polycrystalline Cu was measured by atomic force microscopy (AFM, Figure S1). High-purity Cu (99.998%) purchased from Gredmann Taiwan Ltd. is used as the sputtering target, and Ar^+ serves as the bombardment source. The deposition rate and thickness are monitored using a quartz crystal microbalance. The as-prepared Cu electrode was deposited at a deposition rate of 0.4 Å s^{-1} in the present study.

Preparation of Cyclic Voltammetry (CV)-Treated Cu Electrodes. CV-treated Cu electrode is prepared by cycling the as-prepared Cu electrode in a potential region from 0.55 to −0.3 V. All potentials in the present study are reported with respect to the reversible hydrogen electrode (RHE).

Preparation of Electrodeposited Cu on Au Electrode. A thin Au film with a thickness of ∼10 nm is prepared on a Si prism using electroless deposition described previously.[24,26,33] The Au film was cycled in an Ar-saturated 0.1 M H_2SO_4 solution at a scan rate of 50 mV s^{-1} between 0.1 and 1.6 V (vs RHE) to clean the Au surface.[34] The prepared Au film was then transferred in a solution of 5 mM $CuSO_4$ and 0.1 M H_2SO_4 for the electrochemical deposition process. The Cu film (∼50 nm) was then electrochemically deposited on the Au film at 0.1 V (vs RHE) for 600 s.[26]Figure S2 shows the AFM image and CV of electrodeposited Cu.

In Situ Surface-Enhanced Infrared Absorption Spectroscopy and Electrochemical Measurements. In situ surface-enhanced infrared absorption spectroscopy (SEIRAS) was recorded in the home-built reflection accessory with external reflection configuration using a Thermo Nicolet 6700 FTIR spectrometer equipped with a HgCdTe (MCT) detector.[35] All spectra were acquired with a spectral resolution of 4 cm^{-1}. The typical acquisition time was 30 s per spectrum. The time-dependent measurement takes 12 s per spectrum. For spectroelectrochemical measurements, the spectrometer was coupled with the electrochemical workstation (ZENNIUM E, Zahner). The working electrodes are PVD Cu or electrodeposited Cu on Au. The counter and reference electrodes are graphite rod and Ag/AgCl electrode, respectively. The graphite counter electrode is used to avoid any possible contamination from the Pt electrode.[26] The electrolyte used in all spectroelectrochemical measurements was 0.1 M CO_2-saturated $KHCO_3$ (pH = 6.8). The CV for in situ SEIRAS measurements was performed at a scan rate of 2 mV s^{-1}. Figure S3 shows the cell configuration of in situ SEIRAS measurements. More details for in situ SEIRAS are described elsewhere.[36]

X-ray Absorption Spectroscopy Measurements. In situ soft X-ray absorption spectroscopy was used to monitor the changes in the oxidation state of the Cu surface during reactions. In situ and ex situ Cu L_3-edge X-ray absorption spectroscopy measurements were conducted with total fluorescence yield (TFY) mode and total electron yield (TEY) mode, respectively, in Taiwan Light Source beamline 20A end station (National Synchrotron Radiation Research Center, Taiwan). A flow type spectroelectrochemical cell was used for in situ soft X-ray absorption spectroscopy measurements as described in previous literature.[37] First, we deposit Cu thin film (PVD Cu) with a thickness of ∼36 nm on a SiN_x X-ray transparent window with underlying adhesion layers of Cr (2 nm) and Au (5 nm) serving as the working electrodes, and two Pt wires were used as the counter and reference electrodes. X-ray absorption spectra were collected as a function of applied potential during cyclic voltammetry (CV) at a scan rate of 2 mV s^{-1}, which yields a potential resolution of ∼120 mV owing to an acquisition time of 60 s per spectrum. Figure S4 shows the cell configuration of in situ soft X-ray absorption spectroscopy measurements. Since the Cu electrodes can be easily oxidized under

https://dx.doi.org/10.1021/jacs.9b11126
J. Am. Chem. Soc. 2020, 142, 2857−2867

air conditions, all of the prepared Cu electrodes were kept in a vacuum chamber and transferred to a chamber filled with argon before the soft X-ray absorption spectroscopy measurements to avoid Cu oxidation.

In situ Cu K-edge X-ray absorption spectroscopy including extended X-ray absorption fine-structure spectroscopy (EXAFS) was conducted in the Taiwan Light Source beamline 17A end station (National Synchrotron Radiation Research Center, Taiwan). All of the spectra were further analyzed with Athena software.

Atomic Force Microscopy. The surface morphology of Cu was imaged by atomic force microscopy (AFM, Innova, Bruker) with tapping mode using a Si_3N_4 cantilever (TESPA, radius of 8 nm, spring constant of 42 N m^{-1}, resonance frequency of 320 kHz, Bruker). All AFM studies were conducted on Si prisms with a hemicylindrical holder.

High-Performance Liquid Chromatography and Online Gas Chromatography Measurements. Gas product analysis was carried out using a home-built online gas chromatography (GC) system with a pulsed discharge helium ionization detector (Agilent 7890, USA). The electrochemical cell coupled to the GC system was used to monitor the gas products formed during CO_2 reduction. Figure S5 shows the cell configuration for online GC measurements. High-performance liquid chromatography (HPLC) with a photometric diode array detector (JASCO, Japan) was used to analyze the liquid products such as formic acid (HCOOH). The reaction potential was held for 5 min to accumulate enough product for each GC/HPLC measurement. Each measurement takes ~20 min. Both PVD Cu electrode and electropolished Cu foil were used to study the effect of CV treatment on the product distributions. The electropolished Cu foil was held at −1 V for 60 min to form the as-prepared Cu foil with the oxidation state of Cu(0) in the CO_2-saturated 0.1 M $KHCO_3$ electrolyte. Calculation of the Faradaic efficiencies (FEs) for the gas and liquid products is shown in Supporting Information.

RESULTS AND DISCUSSION

Figure 1a shows the cyclic voltammetry (CV) of the as-prepared Cu electrode and CV-treated Cu electrode with CO_2-saturated 0.1 M $KHCO_3$ electrolyte at a scan rate of 10 mV s^{-1} in the potential range from 0.25 to −1 V. The as-prepared Cu electrode is cycled in the potential region from 0.55 to −0.3 V (inset in Figure 1a). After three cycles, CV-treated Cu electrode is prepared and exhibits a larger reduction current than that of as-prepared Cu electrode in CO_2-saturated 0.1 M $KHCO_3$ electrolyte. Figure 1b and 1c shows the AFM images of the surface morphology of the as-prepared and CV-treated Cu electrodes (after three CV-treated cycles), repectively, with a scanned area of 5 μm × 5 μm. The surface roughness of the CV-treated Cu electrode is similar to that of the as-prepared Cu surface (R_q = 0.44±0.05 nm for the as-prepared Cu surface and R_q = 0.50±0.04 nm for the CV-treated Cu surface), suggesting that the changes in the surface area of the Cu electrode have less contribution on the larger reduction current of the CV-treated Cu surface during CO_2 reduction. Meanwhile, the double-layer capacitances obtained from the Cu electrodes suggest less changes in the surface area of as-prepared Cu after three CV-treated cycles (Figure S6).

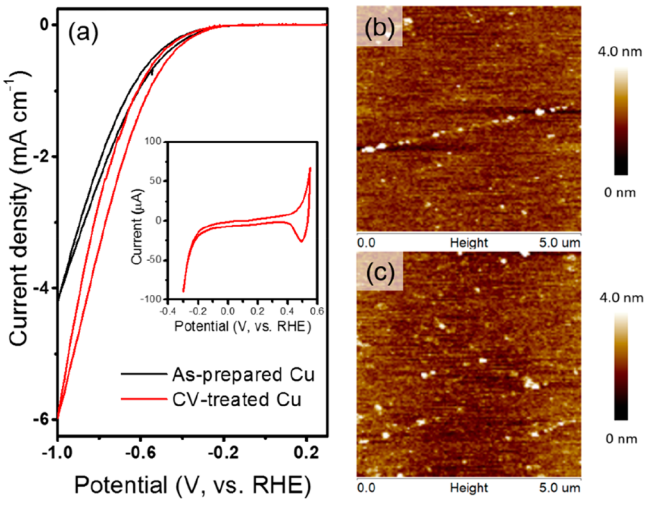


Figure 1. (a) Cyclic voltammetry (CV) of the as-prepared Cu electrode and CV-treated Cu electrode with CO_2-saturated 0.1 M $KHCO_3$ electrolyte at a scan rate of 10 mV s^{-1} in the potential range from 0.25 to −1 V. (Inset) CV curve of the as-prepared Cu electrode obtained in a potential range from −0.3 to 0.55 V. AFM images of the surface morphology of the (b) as-prepared and (c) CV-treated Cu electrodes (after three CV-treated cycles). Scanned area of AFM images is 5 μm × 5 μm.

To study the oxidation state of the different Cu surfaces, ex situ Cu L_3-edge soft X-ray absorption spectroscopy was used to reveal the changes in the oxidation state of the Cu electrode prepared at representative potentials with CO_2-saturated 0.1 M $KHCO_3$ electrolyte. As compared to Cu K-edge hard X-ray absorption spectroscopy, the soft X-ray absorption spectroscopy measurements collected in TEY mode can be used to study the oxidation state of the Cu surface in a range of 2−20 nm thickness which provides surface information.[38,39] Figure 2a shows Cu L_3-edge X-ray absorption spectra (XAS)-TEY mode of Cu, Cu_2O, and CuO electrodes as the reference spectra.[37,40] Peak A at 933.6 eV is associated with the feature of Cu(I), and peak B at 937.5 eV is assigned to the metallic Cu (Cu(0)) in the Cu electrode.[37,40] Figure 2b, 2c, and 2d shows Cu L_3-edge XAS of the as-prepared Cu electrode, CV-treated Cu electrode (after three CV-treated cycles), and electrodeposited Cu electrode in TEY mode, respectively. The feature of peaks A and B suggests that both Cu(0) and Cu(I) exist on the surface of the as-prepared Cu electrode before CO_2 reduction (Figure 2b). Thus, the XAS of the as-prepared Cu electrode also exhibit the Cu(I) feature before CO2RR. The existence of Cu(I) resulting from the surface oxidation of the metallic copper under air conditions prior to immersion in the electrolyte has been proposed previously.[41,42] The XAS of the electrodeposited Cu electrode and CV-treated Cu electrode indicate that Cu(I) dominates the Cu surface before CO2RR and that the Cu(0) feature could be embedded in the spectra. (Figure 2c and 2d)

The prepared Cu electrodes are then held at representative potentials for 10 min during CO_2 reduction. Figure 2b, 2c, and 2d shows that ex situ Cu L_3-edge XAS of the as-prepared Cu electrode, CV-treated Cu electrode, and electrodeposited Cu electrode, respectively, collected in TEY mode were obtained at representative potentials with CO_2-saturated 0.1 M $KHCO_3$ electrolyte. The oxidation state of the as-prepared Cu electrode changes from the mixture of Cu(0) and Cu(I) to Cu(0) at −0.4 V, while the XAS of the other two Cu catalysts are mainly showing the feature of Cu(I). The diminished Cu(I) at lower overpotential could be related to the small amount of Cu(I) in as-prepared Cu electrode. After further reduction at −1 V, the XAS of CV-treated Cu exhibit that the intensity of peak A decreases and the feature of peak B becomes clear after holding the potential at −1 V for 10 min, suggesting that some Cu(I) is reduced to Cu(0) and both Cu(I) and Cu(0) still exist on the Cu surface. In contrast, although the electrodeposited Cu

https://dx.doi.org/10.1021/jacs.9b11126
J. Am. Chem. Soc. 2020, 142, 2857−2867

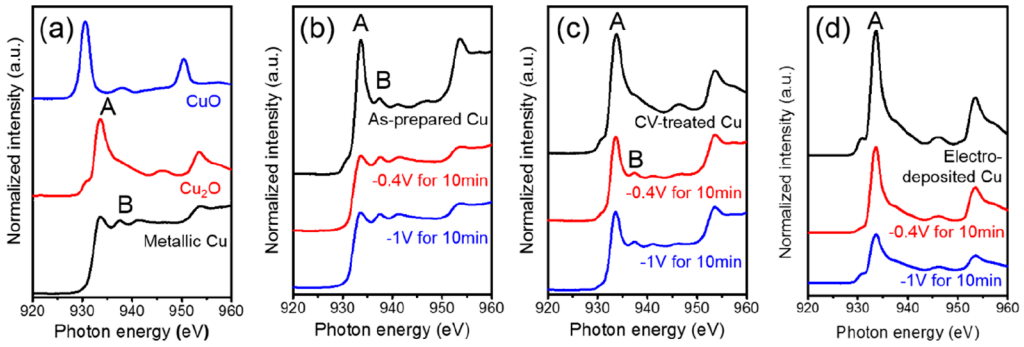


Figure 2. (a) Cu L_3-edge X-ray absorption spectra (XAS)-TEY mode of standard Cu electrodes. Ex situ Cu L_3-edge XAS of the (b) as-prepared Cu electrode, (c) CV-treated Cu electrode (after three CV-treated cycles), and (d) electrodeposited Cu electrode obtained before and after CO_2 reduction. XAS were collected in TEY mode.

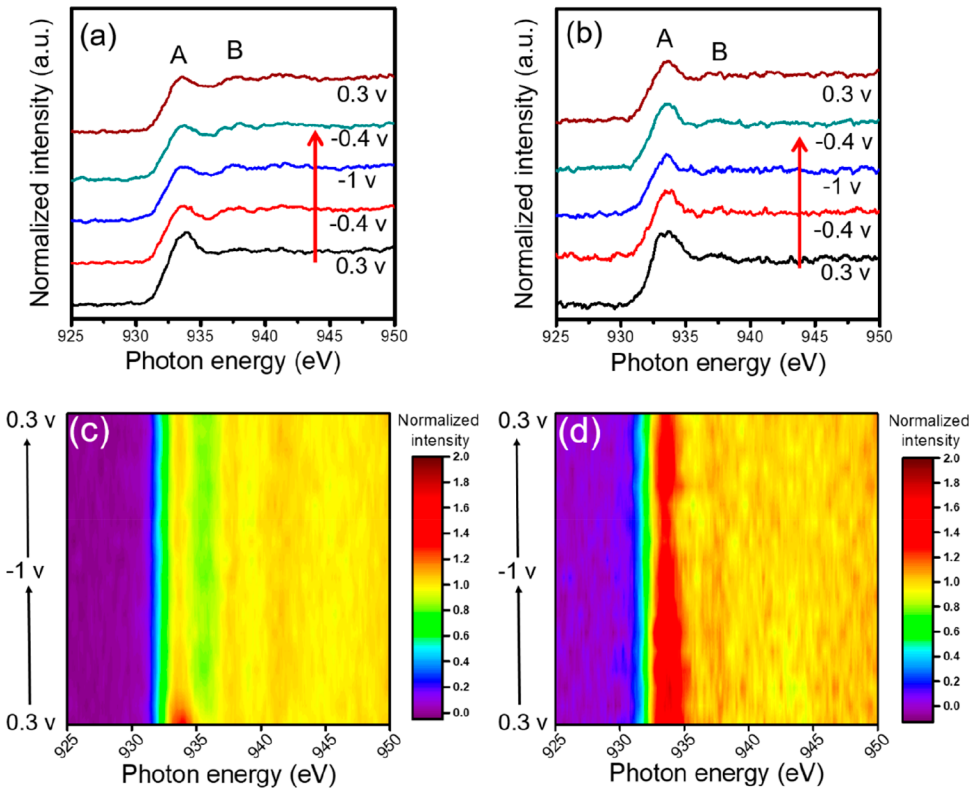


Figure 3. In situ Cu L_3-edge XAS of the (a) as-prepared Cu electrode and (b) CV-oxidized Cu electrode shown at representative potentials with CO_2-saturated 0.1 M $KHCO_3$. Contour plots of in situ Cu L_3-edge XAS of the (c) as-prepared Cu and (d) CV-treated Cu cycled between 0.3 and −1 V. In situ Cu L_3-edge XAS were collected in TFY mode.

should also contain the Cu(0) oxidation state during the reaction, XAS of electrodeposited Cu mainly exhibit the Cu(I) feature after holding the potential at −1 V for 10 min. The reduction from Cu(I) to Cu(0) in electrodeposited Cu electrode takes a longer time than that of the other Cu electrodes, which could be attributed to the larger amount of Cu(I) on the electrodeposited Cu surface.

Hard X-ray absorption spectroscopy (Cu K-edge) was used to characterize the changes in the oxidation state of Cu materials.[18] Figure S7 shows the Cu K-edge XAS of the electrodeposited Cu electrode, as-prepared electrode, and CV-treated Cu electrode. Although Cu K-edge XAS give information about the oxidation state of bulk Cu metal (>2 μm),[43] extended X-ray absorption fine structure (EXAFS) obtained on the as-prepared Cu electrode shows the peak at 2.2 Å which is assigned to the Cu−Cu bond.[44,45] EXAFS of the electrodeposited Cu electrode and CV-treated Cu electrode shows the peak at 1.5 Å associated with a Cu−O bond, suggesting that Cu(I) could result from the persistence of Cu oxides.[18]

To further examine the effect of CV treatment on the characteristics of the Cu electrode during electrochemical CO_2 reduction, we next performed in situ soft X-ray absorption spectroscopy measurements of the as-prepared Cu electrode and CV-treated Cu electrode to reveal the changes in the oxidation state of the Cu surface during electrochemical CO_2 reduction. Although the information provided by the XAS-TEY mode is more surface sensitive, electrochemical soft X-ray absorption measurements can be operated in TFY mode.[46] We show the XAS-TFY mode of standard Cu electrodes in Figure

https://dx.doi.org/10.1021/jacs.9b11126
J. Am. Chem. Soc. 2020, 142, 2857−2867

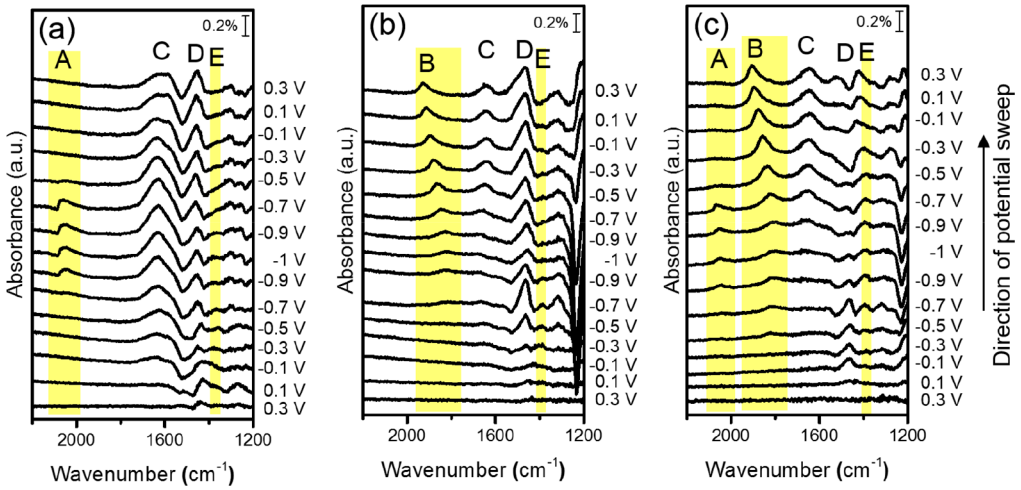


Figure 4. In situ SEIRAS of the (a) electrodeposited Cu electrode, (b) as-prepared Cu electrode, and (c) CV-treated Cu electrode (after three CV-treated cycles) during cathodic (negative) scan and anodic (positive) scan in CO_2-saturated 0.1 M $KHCO_3$ electrolyte.

S8. In situ Cu L_3-edge XAS of the as-prepared Cu electrode shown at representative potentials were obtained in the potential region from 0.3 to −1 V (Figure 3a). The scan rate is 2 mV s^{-1} during cycling, and the electrolyte is CO_2-saturated 0.1 M $KHCO_3$. Peak A at 933.6 eV associated with the feature of Cu(I) appears at 0.3 V.[41] During the CO_2 reduction process, the intensity of peak A decreases during the scan from 0.3 to −1 V, indicating that the oxidation state of the Cu surface changes from Cu(I) to metallic Cu. The oxidation state of the as-prepared Cu electrode persists as Cu(0) during the backward scan from −1 to 0.3 V. In contrast, in situ Cu L_3-edge XAS of the CV-treated Cu (after three CV-treated cycles) still exhibit a combination of Cu(I) and Cu(0) features during cycling (Figure 3b).

Figure 3c and 3d shows the contour plots of the in situ Cu L_3-edge XAS of the as-prepared Cu and CV-treated Cu, respectively, cycled between 0.3 and −1 V with CO_2-saturated 0.1 M $KHCO_3$ electrolyte. In situ Cu L_3-edge XAS of as-prepared Cu show that the intensity of Cu(I) decreases rapidly during the CO_2 reduction process (Figure 3c). In contrast, Figure 3d shows that the feature of Cu(I) obtained at 0.3 V becomes weaker during cycling. We found that the reduction of Cu(I) to Cu(0) in CV-treated Cu is much slower, suggesting that the reduction of the oxidation state over these Cu electrodes is a time-dependent process during CO_2 reduction.

In order to understand the effect of the valence state of the Cu surface on the CO_2 reduction mechanism, we used in situ surface-enhanced infrared absorption spectroscopy (SEIRAS) to identify the intermediates formed on different Cu surfaces during CO_2 reduction. IR spectra were collected every 100 mV during a potential step. All of the IR spectra are shown in Figure S9. Figure 4a, 4b, and 4c shows in situ SEIRA spectra of the electrodeposited Cu electrode, as-prepared Cu electrode, and CV-treated Cu electrode, respectively, obtained at representative potentials during the first cycle. Reference spectra were obtained at 0.3 V in CO_2-saturated 0.1 M $KHCO_3$ electrolyte. Figure 4a shows the in situ SEIRA spectra of the electrodeposited Cu electrode collected in the cathodic (negative) scan from 0.3 to −1 V. Peak A at 2048 cm^{-1} corresponding to atop-adsorbed CO (CO_{atop}) on the Cu surface appears during the negative scan. The asymmetric peak A is observed as the potential is shifted to −1 V.[47] CO_{atop} disappears during the anodic (positive) scan. Among various adsorbed CO species, CO_{atop} is formed alone on the electrodeposited Cu surface during CO_2 reduction.[24,26] The position of the CO_{atop}-associated peak obtained on the Cu surface (2080−2040 cm^{-1}) is different from the position of the CO_{atop}-associated peak obtained on the Au surface (2110−2130 cm^{-1}),[48] suggesting that the electrodeposited Cu electrode completely covers the underlying Au surface.

In contrast, Figure 4b shows the in situ SEIRA spectra of the as-prepared Cu electrode, clearly revealing peak B at 1832 cm^{-1} during negative scan. Peak B associated with bridge-adsorbed CO (CO_{bridge}) on the Cu surface is obtained at −0.5 V and gradually red shifts to 1827 cm^{-1} at −1 V during the negative scan. Upon scanning the potential from −1 to 0.3 V, peak B then blue shifts from 1827 to 1930 cm^{-1}. A similar potential-dependent behavior of the surface-adsorbed CO_{bridge} has been reported on Cu.[27] The blue shift in the vibrational frequency of CO_{bridge} is ascribed to the decrease in the dipole−dipole interaction among CO_{bridge} molecules and/or electron back-donation from the Cu surface to the CO_{bridge} molecules.[27,49] Peak C is associated with the H−O−H bending mode of adsorbed water on the Cu surface, and peak D is assigned to HCO_2^-.[35,50,51] The irreversible changes in the adsorption behavior of adsorbed water during cycling are consistent with previous studies.[35] The role of adsorbed water in the CO_2 reduction mechanism is discussed in the Supporting Information.

Interestingly, in situ SEIRA spectra of the CV-treated Cu electrode show the formation of both CO_{atop} and CO_{bridge} during CO_2 reduction, suggesting that the CO_2 reduction mechanism over the as-prepared Cu surface is changed after the CV treatment (Figure 2c). Although porous Cu materials effectively enhance the vibrational signatures of surface adsorbates, which allows us to probe the surface species,[52] the AFM images of the as-prepared Cu surface and CV-treated Cu surface (after three CV-treated cycles) show a similar roughness of the Cu surfaces and the IR intensities of CO_{bridge}-associated peaks obtained over the two Cu electrodes are the same. Thus, the appearance of CO_{atop} in the CV-treated Cu surface that resulted from the different plasmonic absorption properties of the Cu surface can be excluded. In addition, peak E associated with COO^- is formed, followed by the formation of CO_{atop} and CO_{bridge}. The intensity of peak E decreases in

https://dx.doi.org/10.1021/jacs.9b11126
J. Am. Chem. Soc. 2020, 142, 2857−2867

further reduction. Peak assignments are summarized in Table 1.[24−29,50,51,53,54]

Table 1. Experimental Vibrational Frequencies and Assignments for the Species in Electrochemical CO_2 Reduction

peak label	peak position (cm^{-1})	assignments	ref
A	1951−2094	CO stretching in atop-adsorbed CO	24−29
B	1806−1907	CO stretching in bridge-adsorbed CO	27−29
C	1645	H−O−H bending of H_2O	25,26
D	1467	C−O stretching of HCO_2^-	50,51
E	1396	COO^- symmetric stretching	24,53,54

Figure S10 shows the in situ SEIRA spectrum of the CV-treated Cu electrode obtained at −1 V, exhibiting that both CO_{bridge} and CO_{atop} adsorbed on the Cu surface. We then remove the potential control and replace the electrolyte with fresh CO_2-saturated 0.1 M $KHCO_3$ electrolyte without exposing the Cu electrode to air. On the measured anew SEIRA spectrum of the CV-treated Cu electrode, the CO_{atop}-associated peak disappears. The fact that CO_{atop} can be removed from the surface without the applied potential suggests that the formation of CO_{atop} on the Cu surface is a dynamic adsorption process.

Figure 5a, 5b, and 5c shows the potential dependence of the intensity of CO_{bridge}, CO_{atop}, and COO^- obtained in the electrodeposited Cu electrode, as-prepared Cu electrode, and CV-treated Cu electrode, respectively, from 0.2 to −1 V taken from Figure 4. All peak intensities were normalized to the most intense peak at specific potential. The CO_{atop}-associated peak is observed at −0.6 V and drastically increases from −0.6 to −1 V in the electrodeposited Cu electrode (Figure 5a). The peak associated with COO^- appears at −0.4 V and gradually increases in further reduction. Figure 5b shows that the CO_{bridge}-associated peak appears at −0.4 V in the as-prepared Cu electrode, while the CO_{atop}-associated peak is absent during the CO_2 reduction. Notably, both CO_{bridge}- and CO_{atop}-associated peaks are obtained in the CV-treated Cu electrode, which could be related to the formation of different final products (Figure 5c).

We next study the formation of the CO_{bridge} and CO_{atop} species during continuous cycles. Figure 6a and 6b shows the in situ SEIRA spectra of the as-prepared Cu electrode obtained in the third cycle and the fourth cycle of CO_2 reduction process (after CV-treated cycles), respectively. The reference spectrum is obtained at 0.3 V before the CO_2 reduction. The CO_{bridge}-associated peak resulting from the residual CO_{bridge} on the Cu surface is observed at 0.3 V before the third cycle (Figure 6a). The CO_{bridge}-associated peak red shifts during the negative scan and blue shifts during the backward scan between 0.3 and −1 V, indicating that the adsorption behavior of residual CO_{bridge} is the same during continuous cycles.

Figure 6c shows the potential dependence of the intensity of the CO_{bridge}- and CO_{atop}-associated peaks during four continuous cycles. We found that the growth of residual CO_{bridge} is facilitated by polarizing the potential below −0.5 V during CO_2 reduction. The intensity of the CO_{bridge}-associated peak rises at −0.5 V during the negative scan and keeps increasing during the backward scan until −0.3 V, suggesting that residual CO_{bridge} species is formed on the surface. The total amount of residual CO_{bridge} increases from the first to the third cycle. After CV treatment, the CO_{atop}-associated peak appears during the CO_2 reduction, which could be related to the formation of Cu(I). The intensity of the CO_{bridge}-associated peak drops, suggesting that CO_{bridge} can be removed from the Cu surface during the Cu oxidation process.[27]

Possible reasons for the growth of residual CO_{bridge} during cycles are proposed as follows. (1) The increase in the surface roughness of the Cu electrode could provide more surface area for CO_{bridge} adsorption during cycling. Although AFM images show that the surface roughness of as-prepared Cu electrodes is similar before and after three CV-treated cycles in the potential range from −0.3 to 0.55 V (Figure 1b and 1c), the surface reconstruction of the as-prepared Cu electrode could only take place at the atomic level. In addition, the AFM image of the surface morphology of the CV-treated Cu electrode (after 100 CV-treated cycles) shows that the surface becomes rougher (Figure S11). (2) In situ SEIRA spectra of Cu electrodes show that the peaks associated with the δ_{HOH} bending mode of adsorbed water appear during the negative scan and are maintained during the backward scan,[35] which is most likely due to the irreversible changes of the Cu surface. (3) The increase in the amount of residual CO_{bridge} is similar during each cycle, suggesting that CO_{bridge} species occupy a portion of the Cu surface. The polycrystalline Cu electrode reconstructs and forms Cu (111) and Cu (100) facets in the electrolyte,[55,56] and CO-induced surface reconstruction has been reported.[47] Thus, the irreversible surface reconstruction could lead to formation of more favorable sites for CO_{bridge} adsorption during cycling.

In order to study the persistence of the different CO species during CO_2 reduction, we examined the SEIRA spectra of the CV-treated Cu electrode obtained with time during a holding potential at −0.9 V. Figure 7a shows the in situ SEIRA spectra of the CV-treated Cu electrode and that obtained after holding

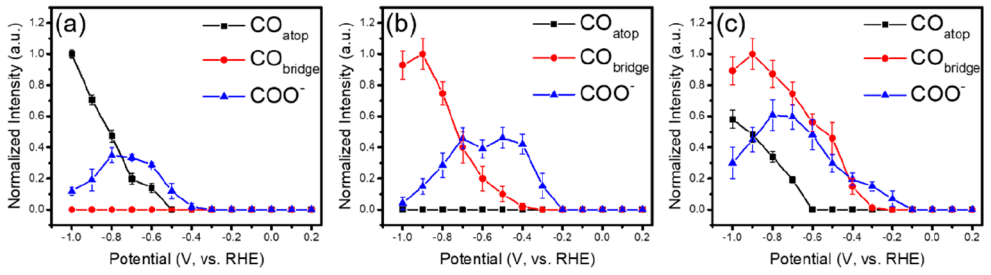


Figure 5. Potential dependence of the intensity of CO_{atop}, CO_{bridge}, and COO^- obtained in the (a) electrodeposited Cu electrode, (b) as-prepared Cu electrode, and (c) CV-treated Cu electrode from 0.2 to −1 V taken from Figure 4.

https://dx.doi.org/10.1021/jacs.9b11126
J. Am. Chem. Soc. 2020, 142, 2857−2867

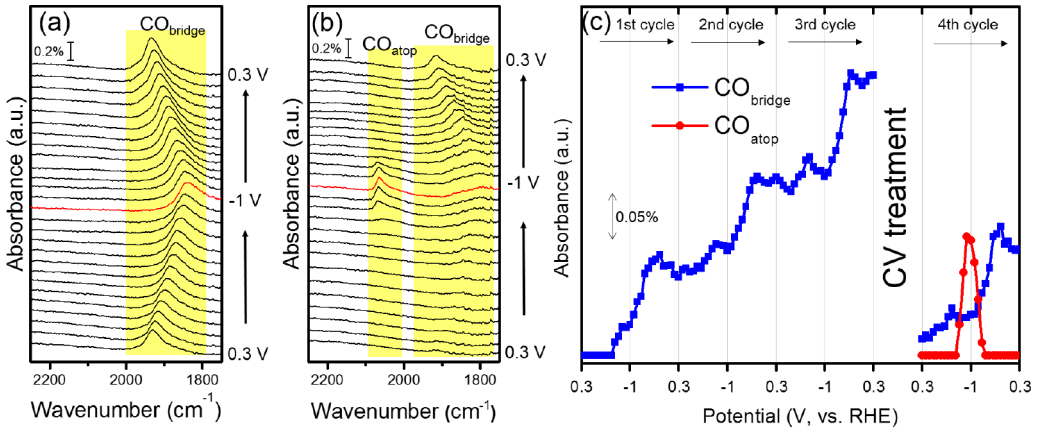


Figure 6. In situ SEIRA spectra of the (a) as-prepared Cu electrode obtained in the (a) third cycle and (b) fourth cycle of the CO_2 reduction process (after CV-treated cycles). (c) Potential dependence of the intensity of the CO_{bridge}- and CO_{atop}-associated peaks during four cycles.

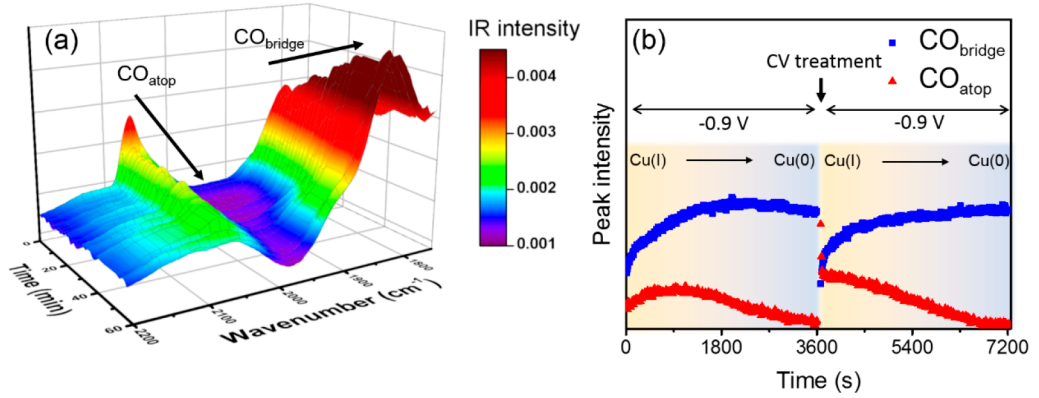


Figure 7. (a) In situ SEIRA spectra of the CV-treated Cu electrode, and (b) time dependence of the CO_{bridge}- and CO_{atop}-associated peak intensities at −0.9 V.

the potential at −0.9 V for 60 min. The CO_{bridge}- and CO_{atop}-associated peaks are absent at 0.3 V, and these peaks appear after stepping the potential from 0.3 to −0.9 V. Figure 7b shows the time dependence of the CO_{bridge}- and CO_{atop}-associated peak intensities at −0.9 V. The intensity of the CO_{bridge}-associated peak reaches a maximum in ∼30 min and remains at −0.9 V. In contrast, the intensity of the CO_{atop}-associated peak increases in the first 15 min and then decreases with time. The decrease in the intensity of CO_{atop} suggests that CO_{atop} leaves the surface easily and CO_{atop} adsorption is a dynamic process. The XAS of the CV-treated Cu electrode obtained during a potential hold at −0.9 V mainly exhibit the Cu(I) feature for the first 15 min, which is due to the slow reduction of Cu(I). After holding the potential at −0.9 V for 60 min, the oxidation state of the Cu surface changes from Cu(I) to Cu(0).

The product distributions obtained from various Cu catalysts were used to examine the electrocatalytic properties of Cu and gain more insight into the CO_2 reduction mechanism. Figure 8 shows the FEs of the major products catalyzed by the electrodeposited Cu electrode, as-prepared Cu electrode, and CV-treated Cu electrode (after 100 CV-treated cycles) at −1 V. The major products catalyzed by the electrodeposited Cu electrode at −1 V are H_2, CH_4, and HCOOH with FEs of 50%, 30%, and 10%, respectively. In addition, only a small amount of C_2 product such as C_2H_4 can be produced at even higher overpotential, which is consistent with previous studies.[25]

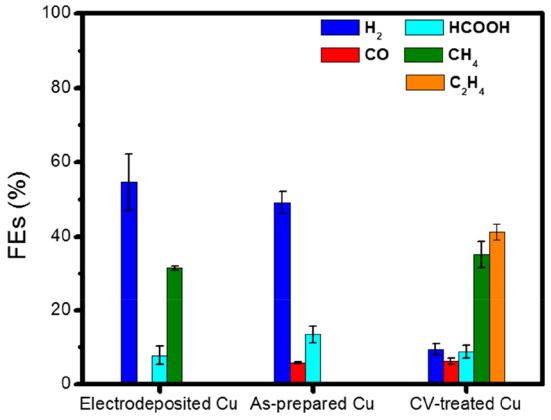
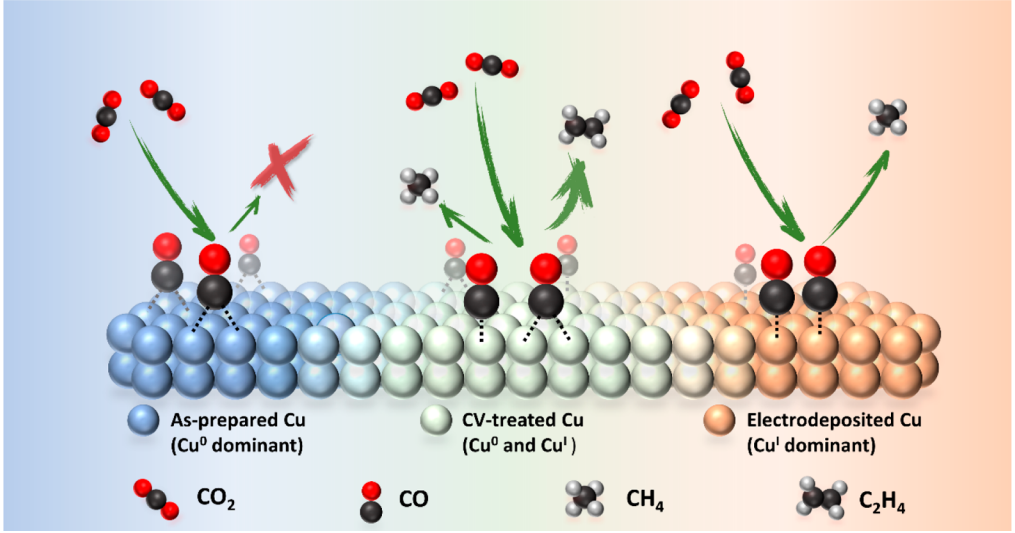


Figure 8. FEs of the major products catalyzed by the electrodeposited Cu electrode, as-prepared Cu electrode, and CV-treated Cu electrode (after 100 CV-treated cycles) at −1 V in CO_2-saturated 0.1 M $KHCO_3$ electrolyte.

The major CO_2 reduction products over the as-prepared Cu electrode are H_2, CO, and HCOOH at −1 V, with the FEs being 50%, 5%, and 10% at −1 V, respectively. H_2 becomes the dominant product, indicating that the high FE toward the hydrogen evolution reaction is observed in the as-prepared Cu electrode and less hydrocarbon products can be formed. In order to provide a significant effect of CV treatment on the final product analysis, the CV-treated Cu electrode is prepared

https://dx.doi.org/10.1021/jacs.9b11126
J. Am. Chem. Soc. 2020, 142, 2857−2867

Scheme 1. Schematic Illustration of the Electrochemical CO_2 Reduction on the Cu Surface



after 100 CV-treated cycles for the online GC measurements. The CV-treated Cu electrode (after 100 CV-treated cycles) produces more hydrocarbon species such as C_2H_4 (FE = 40%) and CH_4 (FE = 35%), suggesting that the presence of CO_{bridge} and CO_{atop} leads to formation of different products. The improved selectivity can be observed even with less CV-treated cycles (Figure S12).

In addition, a similar FE of HCOOH is obtained over the three Cu catalysts at −1 V, suggesting that the oxidation state of Cu and formation of CO species could have less effect on the formation of HCOOH.[13] The lower total FE (~65%) of major products obtained in the as-prepared Cu electrode could result from the formation of residual CO (CO_{bridge}) on the as-prepared Cu surface at −1 V as shown in Figure 7. The CV-treated Cu electrode with the coexistence of Cu(I) and Cu(0) results in the formation of CH_4 and C_2H_4 at −1 V. Both CH_4 (FE = 35%) and C_2H_4 (FE = 40%) are primary CO_2 reduction products, and the FE of H_2 dramatically decreases to ~10%.

We next discuss the possible reasons for the improved CO_2 reduction catalyzed by the CV-treated Cu electrode. Previous studies showed that C_2 products are favored on dendritic or branched copper materials.[11,14] The branched copper oxide nanoparticles exhibited a high FE of ethylene (FE = 70%) and a hydrogen FE of 30% without any byproducts in a neutral aqueous solution.[11] Also, the surface morphology of the Cu electrode has been proposed to change the CO_2 reduction pathway. The surface reorganization of the Cu(polycrystalline) surface to a Cu(polycrystalline)−[Cu(100)] surface is a general phenomenon at a negative potential,[55,56] and the Cu(100) surface requires a lower overpotential to reduce CO_2 to C_2H_4.[57,58] However, the CV-treated Cu electrode exhibits similar surface morphology before and after CO_2 reduction (Figure 1c, Figures S11 and S13). Figure S14 shows that the FEs of the methane and ethylene products catalyzed by the CV-treated Cu electrode (after three CV-treated cycles) decrease with time after holding the potential at −1 V. The decreases in the product selectivity with time are not consistent with surface reorganization of Cu(100) for favorable CO_2-to-ethylene conversion. Moreover, the product distributions obtained in the CV-treated Cu catalysts and dendritic or branched copper materials are different. Thus, the product distributions are not fully correlated with the changes in the surface morphology in the present study.

The role of the Cu oxidation state has been examined in the product selectivity. We prepared Cu electrodes with oxidation states of Cu(0) (i.e., as-prepared Cu electrode) and Cu(I) (i.e., electrodeposited Cu electrode) and a mixture of Cu(0) and Cu(I) (i.e., CV-treated Cu electrode) in the present study. The proposed electrochemical CO_2 reduction mechanism on different Cu catalysts is shown in Scheme 1. In situ SEIRA spectra show that different CO species are formed on these Cu surfaces. The electrodeposited Cu electrode shows that Cu(I) is dominant. The CO_{atop} intermediate species is obtained over the electrodeposited Cu electrode, which could lead to formation of CH_4 as the C_1 product. The residual CO_{bridge} and less hydrocarbon product are obtained in the as-prepared Cu electrode with Cu(0). In the CV-treated Cu electrode, XAS show a combination of the Cu(I) and Cu(0) features. The presence of both CO_{atop} and CO_{bridge} intermediate species on the Cu surface is observed, and formation of C_2 products such as C_2H_4 is enhanced. Although a surface-adsorbed CO_{bridge} has been considered as the irreversible CO species, which is inert to the reduction reaction,[27] our results suggest that CO_{bridge} might play an important role in producing the C_2 products in the presence of CO_{atop}. The quantum mechanics method was used to validate a unique catalyst for electrochemical CO_2 reduction.[23] Xiao et al. proposed that the selectivity and activity of the C_2 products are enhanced at the borders of the oxidized and metallic surface regions.[23] In their proposed model, two CO species including CO_{bridge} and CO_{atop} adsorbed on Cu(0) and Cu(I) regions are negatively and positively charged, respectively, which assist the CO dimerization and form valuable chemical products (HCO_x). Thus, the theoretical model might correlate with the coexistence of CO_{bridge} and CO_{atop} intermediates for improved formation of C_2 product in the CV-treated Cu electrode.

CONCLUSIONS

In summary, we found that the Cu surface with an oxidation state distribution changes the CO_2 reduction mechanism. The electrodeposited Cu electrode shows more Cu(I). The CO_{atop} intermediate species is formed on the surface, and formation of C_1 hydrocarbon product is obtained during further reduction.

https://dx.doi.org/10.1021/jacs.9b11126
J. Am. Chem. Soc. 2020, 142, 2857−2867

The as-prepared Cu electrode exhibits an oxidation state of Cu(0). The CO_{bridge} is formed on the surface and inhibits the formation of hydrocarbon product. In contrast, the CV-treated Cu electrode shows the coexistence of Cu(I) and Cu(0) and forms both CO_{atop} and CO_{bridge} during CO_2 reduction. Enhanced C_2 product selectivity is also obtained. Thus, the oxidation state of the Cu catalysts affects the electrocatalytic properties of the interface and modulates the CO_2 reduction mechanism. Our findings provide a strategy for designing more selective Cu electrocatalysts for electrochemical CO_2 reduction.

■ ASSOCIATED CONTENT

Supporting Information

The Supporting Information is available free of charge at https://pubs.acs.org/doi/10.1021/jacs.9b11126.

AFM images of as-prepared Cu and cross section profile of as-prepared Cu; AFM image and CV of electrodeposited Cu electrode; cell configuration of in situ SEIRAS measurements; cell configuration of in situ soft XAS measurements; cell configuration of online GC measurements; double-layer capacitances of as-prepared Cu electrode and CV-treated Cu electrode; EXAFS spectra of pristine as-prepared, CV-treated, and electrodeposited Cu electrodes; Cu L_3-edge XAS of standard Cu electrodes in TFY mode; in situ SEIRA spectra of electrodeposited Cu electrode, as-prepared Cu electrode, and CV-treated Cu electrodes; in situ SEIRA spectra of CV-treated Cu electrode obtained at −1 V and without applied potential; AFM image of the surface morphology of CV-treated Cu electrode (after 100 CV-treated cycles); FEs of major products catalyzed by CV-treated Cu electrode (after 3, 10, and 30 CV-treated cycles) at −1 V; AFM images of the surface morphology of CV-treated Cu electrode (3 CV-treated cycles) and CV-treated Cu electrode (100 CV-treated cycles) after holding the potential at −1 V for 60 min in the CO_2-saturated 0.1 M $KHCO_3$ electrolyte ; FEs of methane and ethylene catalyzed by CV-treated Cu electrode (after three CV-treated cycles) after holding the potential at −1 V in CO_2-saturated 0.1 M $KHCO_3$ electrolyte (PDF)

■ AUTHOR INFORMATION

Corresponding Author

Heng-Liang Wu − *Center for Condensed Matter Sciences and Center of Atomic Initiative for New Materials, National Taiwan University, Taipei 10617, Taiwan;* orcid.org/0000-0003-1250-9851; Email: hengliangwu@ntu.edu.tw

Authors

Tsu-Chin Chou − *Center for Condensed Matter Sciences, National Taiwan University, Taipei 10617, Taiwan*

Chiao-Chun Chang − *Center for Condensed Matter Sciences, National Taiwan University, Taipei 10617, Taiwan*

Hung-Ling Yu − *Center for Condensed Matter Sciences, National Taiwan University, Taipei 10617, Taiwan*

Wen-Yueh Yu − *Department of Chemical Engineering, National Taiwan University, Taipei 10617, Taiwan;* orcid.org/0000-0001-6818-3075

Chung-Li Dong − *Department of Physics, Tamkang University, New Taipei City 25137, Taiwan;* orcid.org/0000-0002-4289-4677

Juan-Jesús Velasco-Vélez − *Department of Inorganic Chemistry, Fritz-Haber-Institut der Max-Planck-Gesellschaft, Berlin 14195, Germany;* orcid.org/0000-0002-6595-0168

Cheng-Hao Chuang − *Department of Physics, Tamkang University, New Taipei City 25137, Taiwan*

Li-Chyong Chen − *Center for Condensed Matter Sciences and Center of Atomic Initiative for New Materials, National Taiwan University, Taipei 10617, Taiwan*

Jyh-Fu Lee − *National Synchrotron Radiation Research Center, , Hsinchu 30076, Taiwan*

Jin-Ming Chen − *National Synchrotron Radiation Research Center, , Hsinchu 30076, Taiwan*

Complete contact information is available at: https://pubs.acs.org/10.1021/jacs.9b11126

Notes

The authors declare no competing financial interest.

■ ACKNOWLEDGMENTS

This research was funded by MOST (Ministry of Science and Technology), Taiwan (107-2113-M-002-014-MY2). We thank Prof. Tsan-Yao Chen in the Department of Engineering and System Science, National Tsing Hua University, and Prof. Kuan-Wen Wang in the Institute of Materials Science and Engineering, National Central University, for technical support. We thank Ms. Po-Yu Su in the Center for Condensed Matter Sciences, National Taiwan University, for the gas product measurements. We are thankful for the financial support from the Center of Atomic Initiative for New Materials, National Taiwan University, from the Featured Areas Research Center Program within the framework of the Higher Education Sprout Project by the Ministry of Education in Taiwan (108L9008).

■ REFERENCES

(1) Seh, Z. W.; Kibsgaard, J.; Dickens, C. F.; Chorkendorff, I. B.; Norskov, J. K.; Jaramillo, T. F. Combining theory and experiment in electrocatalysis: Insights into materials design. *Science* **2017**, *355*, No. eaad4998.

(2) Zhu, D. D.; Liu, J. L.; Qiao, S. Z. Recent Advances in Inorganic Heterogeneous Electrocatalysts for Reduction of Carbon Dioxide. *Adv. Mater.* **2016**, *28*, 3423.

(3) Kas, R.; Kortlever, R.; Milbrat, A.; Koper, M. T. M.; Mul, G.; Baltrusaitis, J. Electrochemical CO_2 reduction on Cu_2O-derived copper nanoparticles: controlling the catalytic selectivity of hydrocarbons. *Phys. Chem. Chem. Phys.* **2014**, *16*, 12194.

(4) Gao, D.; Aran-Ais, R. M.; Jeon, H. S.; Roldan Cuenya, B. Rational catalyst and electrolyte design for CO_2 electroreduction towards multicarbon products. *Nat. Catal.* **2019**, *2*, 198.

(5) Khezri, B.; Fisher, A. C.; Pumera, M. CO_2 reduction: the quest for electrocatalytic materials. *J. Mater. Chem. A* **2017**, *5*, 8230.

(6) Zheng, Y.; Vasileff, A.; Zhou, X. L.; Jiao, Y.; Jaroniec, M.; Qiao, S. Z. Understanding the Roadmap for Electrochemical Reduction of CO_2 to Multi-Carbon Oxygenates and Hydrocarbons on Copper-Based Catalysts. *J. Am. Chem. Soc.* **2019**, *141*, 7646.

(7) Takahashi, I.; Koga, O.; Hoshi, N.; Hori, Y. Electrochemical reduction of CO_2 at copper single crystal Cu(S)-[n (111) x (111)] and Cu(S)-[n (110) x (100)] electrodes. *J. Electroanal. Chem.* **2002**, *533*, 135.

(8) Hori, Y.; Takahashi, I.; Koga, O.; Hoshi, N. Electrochemical reduction of carbon dioxide at various series of copper single crystal electrodes. *J. Mol. Catal. A: Chem.* **2003**, *199*, 39.

(9) Reske, R.; Mistry, H.; Behafarid, F.; Roldan Cuenya, B.; Strasser, P. Particle Size Effects in the Catalytic Electroreduction of CO_2 on Cu Nanoparticles. *J. Am. Chem. Soc.* **2014**, *136*, 6978.
(10) Cheng, T.; Xiao, H.; Goddard, W. A. Nature of the Active Sites for CO Reduction on Copper Nanoparticles; Suggestions for Optimizing Performance. *J. Am. Chem. Soc.* **2017**, *139*, 11642.
(11) Kim, J.; Choi, W.; Park, J. W.; Kim, C.; Kim, M.; Song, H. Branched Copper Oxide Nanoparticles Induce Highly Selective Ethylene Production by Electrochemical Carbon Dioxide Reduction. *J. Am. Chem. Soc.* **2019**, *141*, 6986.
(12) Jung, H.; Lee, S. Y.; Lee, C. W.; Cho, M. K.; Won, D. H.; Kim, C.; Oh, H. S.; Min, B. K.; Hwang, Y. J. Electrochemical Fragmentation of Cu_2O Nanoparticles Enhancing Selective C-C Coupling from CO_2 Reduction Reaction. *J. Am. Chem. Soc.* **2019**, *141*, 4624.
(13) Gao, D. F.; Zegkinoglou, I.; Divins, N. J.; Scholten, F.; Sinev, I.; Grosse, P.; Roldan Cuenya, B. Plasma-Activated Copper Nanocube Catalysts for Efficient Carbon Dioxide Electroreduction to Hydrocarbons and Alcohols. *ACS Nano* **2017**, *11*, 4825.
(14) Scholten, F.; Sinev, I.; Bernal, M.; Roldan Cuenya, B. Plasma-Modified Dendritic Cu Catalyst for CO_2 Electroreduction. *ACS Catal.* **2019**, *9*, 5496.
(15) Eilert, A.; Cavalca, F.; Roberts, F. S.; Osterwalder, J.; Liu, C.; Favaro, M.; Crumlin, E. J.; Ogasawara, H.; Friebel, D.; Pettersson, L. G. M.; Nilsson, A. Subsurface Oxygen in Oxide-Derived Copper Electrocatalysts for Carbon Dioxide Reduction. *J. Phys. Chem. Lett.* **2017**, *8*, 285.
(16) Dinh, C.-T.; Burdyny, T.; Kibria, M. G.; Seifitokaldani, A.; Gabardo, C. M.; Garcia de Arquer, F. P.; Kiani, A.; Edwards, J. P.; De Luna, P.; Bushuyev, O. S.; Zou, C.; Quintero-Bermudez, R.; Pang, Y.; Sinton, D.; Sargent, E. H. CO_2 electroreduction to ethylene via hydroxide-mediated copper catalysis at an abrupt interface. *Science* **2018**, *360*, 783.
(17) Favaro, M.; Xiao, H.; Cheng, T.; Goddard, W. A.; Yano, J.; Crumlin, E. J. Subsurface oxide plays a critical role in CO_2 activation by Cu(111) surfaces to form chemisorbed CO_2, the first step in reduction of CO_2. *Proc. Natl. Acad. Sci. U. S. A.* **2017**, *114*, 6706.
(18) Mistry, H.; Varela, A. S.; Bonifacio, C. S.; Zegkinoglou, I.; Sinev, I.; Choi, Y. W.; Kisslinger, K.; Stach, E. A.; Yang, J. C.; Strasser, P.; Cuenya, B. R. Highly selective plasma-activated copper catalysts for carbon dioxide reduction to ethylene. *Nat. Commun.* **2016**, *7*, 12123.
(19) Li, C. W.; Kanan, M. W. CO_2 Reduction at Low Overpotential on Cu Electrodes Resulting from the Reduction of Thick Cu_2O Films. *J. Am. Chem. Soc.* **2012**, *134*, 7231.
(20) Eilert, A.; Roberts, F. S.; Friebel, D.; Nilsson, A. Formation of Copper Catalysts for CO_2 Reduction with High Ethylene/Methane Product Ratio Investigated with *In Situ* X-ray Absorption Spectroscopy. *J. Phys. Chem. Lett.* **2016**, *7*, 1466.
(21) Mariano, R. G.; McKelvey, K.; White, H. S.; Kanan, M. W. Selective increase in CO_2 electroreduction activity at grain-boundary surface terminations. *Science* **2017**, *358*, 1187.
(22) Feng, X. F.; Jiang, K. L.; Fan, S. S.; Kanan, M. W. Grain-Boundary-Dependent CO_2 Electroreduction Activity. *J. Am. Chem. Soc.* **2015**, *137*, 4606.
(23) Xiao, H.; Goddard, W. A.; Cheng, T.; Liu, Y. Y. Cu metal embedded in oxidized matrix catalyst to promote CO_2 activation and CO dimerization for electrochemical reduction of CO_2. *Proc. Natl. Acad. Sci. U. S. A.* **2017**, *114*, 6685.
(24) Heyes, J.; Dunwell, M.; Xu, B. J. CO_2 Reduction on Cu at Low Overpotentials with Surface-Enhanced *in Situ* Spectroscopy. *J. Phys. Chem. C* **2016**, *120*, 17334.
(25) Wuttig, A.; Liu, C.; Peng, Q. L.; Yaguchi, M.; Hendon, C. H.; Motobayashi, K.; Ye, S.; Osawa, M.; Surendranath, Y. Tracking a Common Surface-Bound Intermediate during CO_2-to-Fuels Catalysis. *ACS Cent. Sci.* **2016**, *2*, 522.
(26) Zhu, S. Q.; Jiang, B.; Cai, W. B.; Shao, M. H. Direct Observation on Reaction Intermediates and the Role of Bicarbonate Anions in CO_2 Electrochemical Reduction Reaction on Cu Surfaces. *J. Am. Chem. Soc.* **2017**, *139*, 15664.
(27) Gunathunge, C. M.; Ovalle, V. J.; Li, Y. W.; Janik, M. J.; Waegele, M. M. Existence of an Electrochemically Inert CO Population on Cu Electrodes in Alkaline pH. *ACS Catal.* **2018**, *8*, 7507.
(28) Malkani, A. S.; Dunwell, M.; Xu, B. J. Operando Spectroscopic Investigations of Copper and Oxide Derived Copper Catalysts for Electrochemical CO Reduction. *ACS Catal.* **2019**, *9*, 474.
(29) Hayden, B. E.; Kretzschmar, K.; Bradshaw, A. M. An Infrared Spectroscopic Study of CO on Cu(111) - the Linear, Bridging and Physisorbed Species. *Surf. Sci.* **1985**, *155*, 553.
(30) Salimon, J.; Hernandez-Romero, R. M.; Kalaji, M. The dynamics of the conversion of linear to bridge bonded CO on Cu. *J. Electroanal. Chem.* **2002**, *538*, 99.
(31) Ooka, H.; Figueiredo, M. C.; Koper, M. T. M. Competition between Hydrogen Evolution and Carbon Dioxide Reduction on Copper Electrodes in Mildly Acidic Media. *Langmuir* **2017**, *33*, 9307.
(32) Wang, H.-F.; Yan, Y.-G.; Huo, S.-J.; Cai, W.-B.; Xu, Q.-J.; Osawa, M. Seeded growth fabrication of Cu-on-Si electrodes for *in situ* ATR-SEIRAS applications. *Electrochim. Acta* **2007**, *52*, 5950.
(33) Lee, S.; Lee, J. Ethylene Selectivity in CO Electroreduction when using Cu Oxides: An *In Situ* ATR-SEIRAS Study. *ChemElectroChem* **2018**, *5*, 558.
(34) Yaguchi, M.; Uchida, T.; Motobayashi, K.; Osawa, M. Speciation of Adsorbed Phosphate at Gold Electrodes: A Combined Surface-Enhanced Infrared Absorption Spectroscopy and DFT Study. *J. Phys. Chem. Lett.* **2016**, *7*, 3097.
(35) Ataka, K.; Yotsuyanagi, T.; Osawa, M. Potential-dependent reorientation of water molecules at an electrode/electrolyte interface studied by surface-enhanced infrared absorption spectroscopy. *J. Phys. Chem.* **1996**, *100*, 10664.
(36) Chen, Y. X.; Miki, A.; Ye, S.; Sakai, H.; Osawa, M. Formate, an active intermediate for direct oxidation of methanol on Pt electrode. *J. Am. Chem. Soc.* **2003**, *125*, 3680.
(37) Velasco-Velez, J.-J.; Jones, T.; Gao, D.; Carbonio, E.; Arrigo, R.; Hsu, C.-J.; Huang, Y.-C.; Dong, C.-L.; Chen, J.-M.; Lee, J.-F.; Strasser, P.; Roldan Cuenya, B.; Schlogl, R.; Knop-Gericke, A.; Chuang, C.-H. The Role of the Copper Oxidation State in the Electrocatalytic Reduction of CO_2 into Valuable Hydrocarbons. *ACS Sustainable Chem. Eng.* **2019**, *7*, 1485.
(38) Degroot, F. M. F. X-Ray-Absorption and Dichroism of Transition-Metals and Their Compounds. *J. Electron Spectrosc. Relat. Phenom.* **1994**, *67*, 529.
(39) Achkar, A. J.; Regier, T. Z.; Wadati, H.; Kim, Y. J.; Zhang, H.; Hawthorn, D. G. Bulk sensitive X-ray absorption spectroscopy free of self-absorption effects. *Phys. Rev. B: Condens. Matter Mater. Phys.* **2011**, *83*, 081106.
(40) Velasco-Velez, J. J.; Skorupska, K.; Frei, E.; Huang, Y. C.; Dong, C. L.; Su, B. J.; Hsu, C. J.; Chou, H. Y.; Chen, J. M.; Strasser, P.; Schlogl, R.; Knop-Gericke, A.; Chuang, C. H. The Electro-Deposition/Dissolution of $CuSO_4$ Aqueous Electrolyte Investigated by In Situ Soft X-ray Absorption Spectroscopy. *J. Phys. Chem. B* **2018**, *122*, 780.
(41) Lien, H. T.; Wong, D. P.; Tsao, N. H.; Huang, C. I.; Su, C. C.; Chen, K. H.; Chen, L. C. Effect of Copper Oxide Oxidation State on the Polymer-Based Solar Cell Buffer Layers. *ACS Appl. Mater. Interfaces* **2014**, *6*, 22445.
(42) Hollmark, H. M.; Vegelius, J. R.; Kristiansen, P.; Werme, L.; Duda, L. C. Exposure of Oxidized Copper Surfaces to Aqueous Na_2S Solution Studied with Soft X-Ray Spectroscopy. *J. Electrochem. Soc.* **2011**, *158*, C1.
(43) Stern, E. A.; Kim, K. Thickness Effect on the Extended-X-Ray-Absorption-Fine-Structure Amplitude. *Phys. Rev. B: Condens. Matter Mater. Phys.* **1981**, *23*, 3781.
(44) Wang, X. T.; Martin, N. M.; Nilsson, J.; Carlson, S.; Gustafson, J.; Skoglundh, M.; Carlsson, P. A. Copper-Modified Zeolites and Silica for Conversion of Methane to Methanol. *Catalysts* **2018**, *8*, 545.
(45) Weng, Z.; Wu, Y. S.; Wang, M. Y.; Jiang, J. B.; Yang, K.; Huo, S. J.; Wang, X. F.; Ma, Q.; Brudvig, G. W.; Batista, V. S.; Liang, Y. Y.; Feng, Z. X.; Wang, H. L. Active sites of copper-complex catalytic

https://dx.doi.org/10.1021/jacs.9b11126
J. Am. Chem. Soc. 2020, 142, 2857−2867

materials for electrochemical carbon dioxide reduction. *Nat. Commun.* **2018**, *9*, 415.
(46) Ruosi, A.; Raisch, C.; Verna, A.; Werner, R.; Davidson, B. A.; Fujii, J.; Kleiner, R.; Koelle, D. Electron sampling depth and saturation effects in perovskite films investigated by soft x-ray absorption spectroscopy. *Phys. Rev. B: Condens. Matter Mater. Phys.* **2014**, *90*, 125120.
(47) Gunathunge, C. M.; Li, X.; Li, J. Y.; Hicks, R. P.; Ovalle, V. J.; Waegele, M. M. Spectroscopic Observation of Reversible Surface Reconstruction of Copper Electrodes under CO_2 Reduction. *J. Phys. Chem. C* **2017**, *121*, 12337.
(48) Sun, S. G.; Cai, W. B.; Wan, L. J.; Osawa, M. Infrared absorption enhancement for CO adsorbed on Au films in perchloric acid solutions and effects of surface structure studied by cyclic voltammetry, scanning tunneling microscopy, and surface-enhanced IR spectroscopy. *J. Phys. Chem. B* **1999**, *103*, 2460.
(49) Samjeske, G.; Komatsu, K.; Osawa, M. Dynamics of CO Oxidation on a Polycrystalline Platinum Electrode: A Time-Resolved Infrared Study. *J. Phys. Chem. C* **2009**, *113*, 10222.
(50) Iwasita, T.; Nart, F. C.; Lopez, B.; Vielstich, W. On the Study of Adsorbed Species at Platinum from Methanol, Formic-Acid and Reduced Carbon-Dioxide Via *Insitu* Ft-Ir Spectroscopy. *Electrochim. Acta* **1992**, *37*, 2361.
(51) Figueiredo, M. C.; Ledezma-Yanez, I.; Koper, M. T. M. *In Situ* Spectroscopic Study of CO_2 Electroreduction at Copper Electrodes in Acetonitrile. *ACS Catal.* **2016**, *6*, 2382.
(52) Osawa, M.; Ataka, K.; Yoshii, K.; Nishikawa, Y. Surface-Enhanced Infrared-Spectroscopy - The Origin of the Absorption Enhancement and Band Selection Rule in the Infrared-Spectra of Molecules Adsorbed on Fine Metal Particles. *Appl. Spectrosc.* **1993**, *47*, 1497.
(53) Lee, S. J.; Han, S. W.; Yoon, M.; Kim, K. Adsorption characteristics of 4-dimethylaminobenzoic acid on silver and titania: Diffuse reflectance infrared Fourier transform spectroscopy study. *Vib. Spectrosc.* **2000**, *24*, 265.
(54) Firet, N. J.; Smith, W. A. Probing the Reaction Mechanism of CO_2 Electroreduction over Ag Films via Operando Infrared Spectroscopy. *ACS Catal.* **2017**, *7*, 606.
(55) Kim, Y. G.; Baricuatro, J. H.; Javier, A.; Gregoire, J. M.; Soriaga, M. P. The Evolution of the Polycrystalline Copper Surface, First to Cu(111) and Then to Cu(100), at a Fixed CO_2RR Potential: A Study by Operand EC-STM. *Langmuir* **2014**, *30*, 15053.
(56) Kim, Y.-G.; Baricuatro, J. H.; Soriaga, M. P. Surface Reconstruction of Polycrystalline Cu Electrodes in Aqueous KHCO3 Electrolyte at Potentials in the Early Stages of CO2 Reduction. *Electrocatalysis* **2018**, *9*, 526.
(57) Huang, Y.; Handoko, A. D.; Hirunsit, P.; Yeo, B. S. Electrochemical Reduction of CO2 Using Copper Single-Crystal Surfaces: Effects of CO* Coverage on the Selective Formation of Ethylene. *ACS Catal.* **2017**, *7*, 1749.
(58) Schouten, K. J.; Qin, Z.; Perez Gallent, E.; Koper, M. T. Two pathways for the formation of ethylene in CO reduction on single-crystal copper electrodes. *J. Am. Chem. Soc.* **2012**, *134*, 9864.

https://dx.doi.org/10.1021/jacs.9b11126
J. Am. Chem. Soc. 2020, 142, 2857−2867